

VORTEX MOTIONS IN THE ATMOSPHERIC CONVECTIVE BOUNDARY LAYER*

Sang Jianguo (桑建国) and Zhang Zhikun (张治坤)

Department of Geophysics, Peking University, Beijing 100871

Received March 17, 1998

ABSTRACT

Large vortices with scales ranging from hundreds meters to tens of kilometers are generally found in the atmospheric convective boundary layer (CBL).

These vortices play important roles in the vertical transport of momentum, heat, water vapor and other tracers in the boundary layer. On the basis of the view of interaction between the convection in CBL and the gravity waves in the upper stable layer the authors developed a convection-wave theory on the formation of large vortices. According to the theory the wavenumber spectrum of the large vortices mainly depends on the atmospheric conditions in both of the upper and lower layers, such as wind speed, wind direction shear, stratification as well as temperature jump.

In the present paper satellite image and weather data in a case of cold air outbreak over warm ocean are analyzed to study every stage of the convective processes, such as cloud street, convective cell as well as their transformation. According to the theory the wavenumber compositions for cloud street and convective cell are calculated, respectively, on the basis of the atmospheric conditions at every stage. The distributions of vertical motions, convergent band and disturbed interface are obtained and compared with the cloud patterns in the convective processes.

Thus the study seems to offer a likely explanation for the origin of large vortices in CBL.

Key words: convection wave theory, large vortex, cloud street, convective cell

I. INTRODUCTION

The convective boundary layer (CBL) plays important roles in the earth-atmosphere interaction. Observations show that the values of momentum flux, heat flux as well as water vapor flux in CBL are tens or hundreds times as much as that in stable boundary layer. One of the significant features in CBL is the large vortex structure. Satellite pictures show that over the ocean surface the large vortices often appear as the form of cloud streets or mesoscale cellular convection (MCC), specially during cold air outbreaks over the warm ocean surface. The cloud streets consist of roll vortices in alignment with the mean wind direction in CBL. In the updraft region of the rolls the cloud bands parallel to each others appear. The roll vortices have the following characteristics. Their depth, h , is 1 to 2 km, horizontal wavelength, λ , is 2 to 20 km with aspect ratio, λ/h , of 2 to 15. The angle, α , between the roll axis and the mean wind ranges from -20° to $+30^\circ$. While MCC consists of open or closed cloud clusters shaped like polygon with diameter of 10 to

* This research was supported by the National Natural Science Foundation of China.

100 km. They often appear downwind of the cloud streets and are gradually transformed from the widening cloud streets. The cloud streets with identical patterns over vast ocean surface are hardly found over land because of the inhomogeneity of the land surface. However, similar roll vortices can still occur over land surface as organized thermals. The vertical velocity in roll vortices has values of 1 to 3 m s⁻¹. Thus the roll vortices are more efficient in the vertical transport of momentum, heat, water vapor as well as other trace elements than the conventional small-scale turbulence.

Since the great significance of the large vortex structure in the studies of CBL several extensive observations have been carried out since 1970s such as BOMEX (see Crossman 1982), MASEX (Chou et al. 1986), KonTur (Brummer 1985) and GATE (Chou and Ferguson 1991) over oceans; PHOENIX (Young 1988) and Convection Waves Project of NCAR (Kuettner et al. 1987) over land. In these observations in addition to satellite pictures, airplanes, Doppler radars and meteorological towers were also used. The observations demonstrated that the large vortex as a multiscale phenomenon plays significant role in the processes of mixing, flux transport and entrainment in CBL. The airplane observation in Convection Waves Project showed that the gravity waves, so-called convection waves, in stable free atmosphere induced by the convective activities in CBL might extend to be close to tropopause.

In the theoretical studies three hypotheses, inflexion instability (Drazin and Reid 1981), parallel instability (Lilly 1966) and convective instability (Agee 1987), derived from the viewpoint that the instability of mean flow may be induced by mechanical or thermal forcing, have been developed to explain the origin of the large vortex. Among them the inflexion instability proves that shear flow with maximum vorticity may produce the vortex with declination angle of $\alpha=14^\circ$ and aspect of $\lambda/h=3$; while parallel instability shows that the shear of mean flow may induce vortex with $\alpha=15^\circ$ and $\lambda/h=6$. The convective instability with Rayleigh number as a criterion illustrates that thermal instability may bring about vortex motion with $\lambda/h=2$. All the theories above can explain neither the variety of aspect ratios of the vortices nor the transition processes from cloud streets to convective cells. A review paper (Etling and Brown 1993) on roll vortex held that the theories above can not be regarded as the universal mechanism of the roll vortex since they can only explain the origin of individual roll vortex and can hardly make clear the multiscale processes of the roll vortex.

Proceeding with the consideration of interaction between the convection in the unstable boundary layer and the gravity waves in the upper stably overlying layer, the authors have recently developed the convection wave theory of the structure of the large roll vortex (Sang 1991; 1993). The theory demonstrates that a thermal disturbance in the boundary layer, for instance an intense thermal, penetrates into the upper stable layer and stimulates gravity waves there. The horizontally propagating trapped waves in turn bring out and tune up the convective activities and make them into large organized vortices. Based on the analytical solutions of two-layer model for the linearized atmospheric wave equation, the theory proves that the wavenumber composition of the roll vortex is controlled by the factors in the boundary layer and the upper stable layer such as stratification, wind speed and direction shear, boundary layer depth as well as temperature

jump at the top of boundary layer.

In the paper based on the convection-wave theory a convective process induced by cold air outbreaks over warm ocean surface will be analyzed. Satellite pictures showed that this convective process could be temporally divided into several phases such as the convective streets over ocean, the transition into cells, the decline of convection over ocean and the reestablishment of convection as entry of cold air into warm land surface. In the following the characteristics of the vortices in the lower atmosphere in each phase of the convective process will be studied respectively.

II. CONVECTION-WAVE THEORY ON STRUCTURE OF THE LARGE ROLL VORTEX

By assuming that the vortex motion in the atmosphere consists of disturbance components with different wavenumber, the vertical velocity induced by the disturbances can be expressed as

$$w(x, y, z) = \int_{-\infty}^{\infty} \int_0^{\infty} \tilde{w}(k, l, z) e^{ikx} e^{ily} dk dl, \tag{1}$$

where k and l are the wavenumber in X and Y axes respectively, \tilde{w} represents the component with wavenumber of k and l . In an irrotational and inviscid atmosphere the component \tilde{w} follows the equation (see Sang 1993)

$$\frac{\partial^2 \tilde{w}}{\partial z^2} + \left\{ \frac{k^2 + l^2}{U^2 (k + \alpha l)^2} \beta g - (k^2 + l^2) \right\} \tilde{w} = F(k, l, z), \tag{2}$$

where F in the right-hand side of the equation represents the forcing term concerning mechanical or thermal disturbance: $\beta = (1/\theta) (\partial \theta / \partial z)$. $\alpha = V/U$. U and V are the wind speed components in X and Y directions respectively, where X is taken as the direction of mean wind in the boundary layer.

The atmosphere is divided into two layers where the lower one is the convective layer with $\beta_1 < 0$, and the upper one is stable with $\beta_2 > 0$. The interface between the two layers is assumed to be continuous for speed and discontinuous for density or potential temperature.

Giving a dynamic disturbance source, a hill for instance, or a thermal disturbance source, a strong thermal for instance, solving Eq. (2) to obtain \tilde{w} , and putting it into Eq. (1), we have (Sang 1991; 1993):

$$w(x, y, z) = \text{Re} \left[\iint \frac{M e^{-ak} e^{-bl} e^{ikx} e^{ily} \sinh(\lambda z)}{\lambda \cosh(\lambda h) - \left(\frac{k^2 + l^2}{k^2} \gamma - \mu \right) \sinh(\lambda h)} dk dl \right], \tag{3}$$

where M is a parameter representing the strength of disturbance source; a and b are the horizontal scales of disturbance source in X and Y directions respectively; h is the depth of the boundary layer: $\lambda^2 = (k^2 + l^2) (k^2 + n^2) / k^2$ and $\mu^2 = (k^2 + l^2) [1 - m^2 / (k + \alpha l)^2]$, n and m are the stability parameters in the lower and upper layers respectively, $n^2 = -g\beta_1 / U_1^2$ and $m^2 = g\beta_2 / U_2^2$; U_1 , U_2 , θ_1 and θ_2 are the mean speed and potential temperature in the two layers; $\gamma = (g/U^2) (\Delta\theta/\theta)$ is the parameters representing the temperature jump at the interface; $\alpha = V_2/U_2$ representing the angle between the wind directions in the upper layer and the lower layer.

It can be seen from Eq. (3) that not all wavenumber components make contribution to the integral. Only the components with wavenumbers k and l making the denominator zero can exert influences on the vortex motion. Thus we have the wavenumber selection relation

$$\lambda \cosh(\lambda h) - \left(\frac{k^2 + l^2}{k^2} \gamma - \mu \right) \sinh(\lambda h) = 0. \quad (4)$$

The nonlinear transcendental equation (4) can be solved with Newton method. For given values of atmospheric parameters m , n , h , γ and α , an appropriate value of l corresponding to each given value of k is obtained by solving Eq. (4). see Fig. 3. Each pair of wavenumbers (k, l) represents a resonant component of the wave motion. This indicates that the energy spectrum of the disturbances is distributed along a line on (k, l) plane, that is the so-called line spectrum. The wavenumber selection relation (4) shows that the wavenumber composition (k, l) of the disturbance induced by the interaction between the convection in the boundary layer and the waves in the upper stable layer is determined by the atmospheric conditions in the upper and lower layers, represented by the parameters m , n , h , γ and α . These parameters control the downwind and cross-wind wavelengths $L_x = 2\pi/k$ and $L_y = 2\pi/l$ and thus define the pattern of the vortex motion.

Equation (3) can be solved with residue theorem

$$w = \begin{cases} \int_{k_c}^{\infty} \frac{Me^{-ak}e^{-bl}\lambda}{G(k, l)} \frac{\sin\{\lambda(h+z)\}}{\sinh(\lambda h)} \sin(kx+ly) dk, & \text{as } z \leq h \text{ (lower layer)} \\ \int_{k_c}^{\infty} \frac{Me^{-ak}e^{-bl}\lambda}{G(k, l)} e^{-\mu z} \sin(kx+ly) dk, & \text{as } z > h \text{ (upper layer)} \end{cases} \quad (5)$$

where $G(k, l) = \frac{\partial}{\partial t} \left\{ \lambda \cosh(\lambda h) - \left(\frac{k^2 + l^2}{k^2} \gamma - \mu \right) \sinh(\lambda h) \right\}$. In Eq. (5) the lower limit k_c of the integral is the cutoff wavenumber of the trapped waves. In addition to Eq. (4), another restrictive condition of the cutoff wavenumbers is

$$(k_c + \alpha l_c)^2 = m^2. \quad (6)$$

As $k \geq k_c$ and $l \geq l_c$ the parameter μ is real and thus the waves in the upper layer decline with height. Then the waves are confined in the lower layer and propagate downstream.

Since Expression (5) includes the factors e^{-ak} and e^{-bl} , the contribution to the integral by the wavenumber components decreases rapidly with k and l . Thus the disturbance induced by the convection waves consist of the wavenumber components starting with the cutoff wavenumber (k_c, l_c) . The wavenumber composition defines the shape, orientation and strength of the disturbances. According to the different atmospheric conditions the disturbances may present different appearances such as streets or cells.

III. SYNOPTIC ANALYSES OF THE LARGE VORTEX STRUCTURE

The authors have analysed the synoptic data and satellite pictures of ten cases of convective vortices caused by cold air outbreaks over warm ocean surface. As space is limited only one case study is presented as follows.

Figure 1 is composed of two successive satellite pictures at 1553 and 1410 GMT, March 11, 1982, in channel 0.725–1.1 μm of NOAA Satellite (see Scorer 1986). This figure shows the convective cloud streets and cells over the North Atlantic Ocean caused

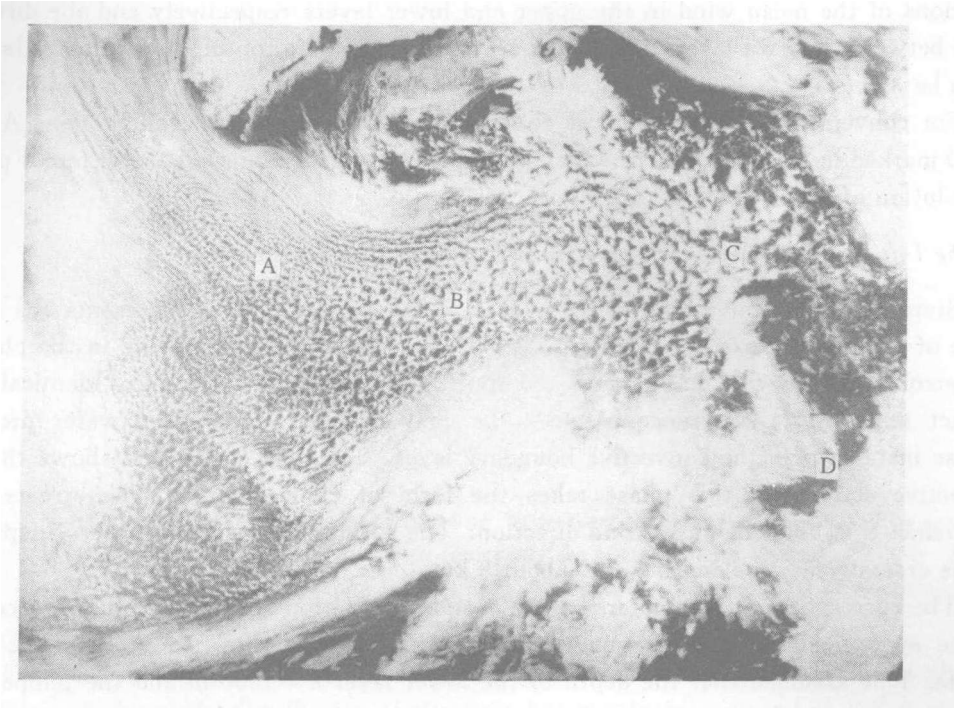


Fig. 1. Satellite picture at 1553 and 1410 GMT. March 11, 1982.

by cold air outbreaks, which broke out from Arctic ice cap, passed Davis strait and flowed around the south end of Greenland. Figure 2 is the synoptic map of 850 hPa at 0000 GMT of the same day. The temperature difference and the depth between 850 hPa and the surface as well as between 700 hPa and 850 hPa can be taken as the measures of the stability in the boundary layer and the upper stable layer. The wind direction and the orientation of the contour lines in 850 hPa, 700 hPa and the surface represent the

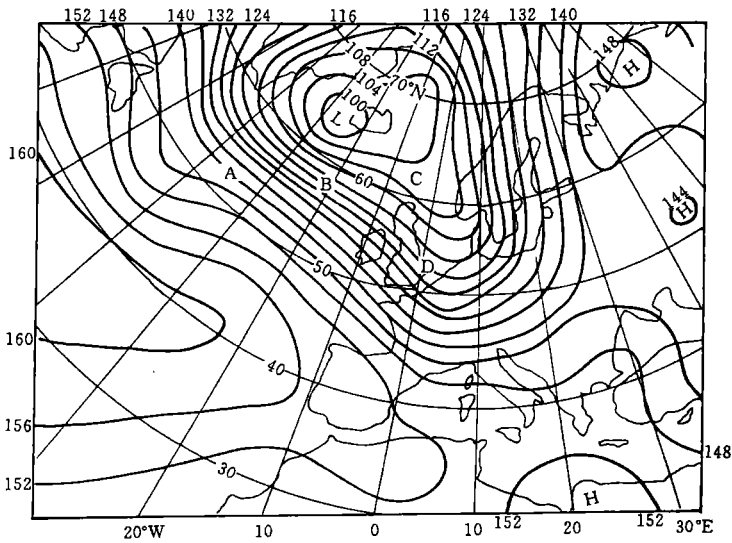


Fig. 2. Synoptic map of 850 hPa at 0000 GMT. March 11, 1982.

directions of the mean wind in the upper and lower layers respectively and the direction shear between the two layers. The temperature jump at the top of the boundary layer is set to be 3°C .

For convenience the atmospheric conditions and the cloud forms in Stations A, B, C and D marked in Figs. 1 and 2 are taken as examples, which represent the different phases of evolution of the convective process.

1. *The Initial Phase of Convective Activity—Convective Cloud Streets*

Station A, located at the ocean surface south of Greenland, represents the initial phase of cold air outbreaks. It can be seen in Figs. 1 and 2 that the wind in the phase is very strong and the wind directions in the upper and lower layers are almost identical. The distinct temperature difference between the cold air and warm ocean water produces intense instability in the convective boundary layer. The satellite picture shows that the convective activity in this phase takes the form of cloud streets. The streets align approximately along the mean wind direction. The spacing between the streets, expressed by the cross-wind wavelength L_y , is about 8 km.

The corresponding parameters n , m , γ , α and h in Station A can be evaluated according to the synoptic data and the general characteristics of shallow convection like cloud streets. It is assumed that the depth of the lower layer $h=1000$ m and the temperature jump at the top of the boundary layer $\Delta\theta=3^{\circ}\text{C}$, whose usual values range 2 to 5°C . According to the temperature (280 and 272 K respectively) and the height at 700 hPa and 850 hPa, the potential temperature gradient in the upper layer is $\partial\theta_2/\partial z=-0.005$ K m^{-1} . Based on this value and the temperature jump the potential temperature at the top can be estimated to be 267 K (see Fig. 11).

According to the surface temperature and the potential temperature at the top of boundary layer the potential temperature gradient in the lower layer is about $\partial\theta_1/\partial z=-0.0046$ K m^{-1} . Since the wind speeds at the surface, 850 hPa and 700 hPa are 16, 16 and 24 m s^{-1} respectively, therefore $U_1=16$ m s^{-1} and $U_2=24$ m s^{-1} . From the expressions of n^2 and m^2 it is obtained that $n=0.0007$ m^{-1} and $m=0.0005$ m^{-1} . According to the wind speeds, directions and the orientation of the contours at each level it is estimated that $\alpha=0.1$. Similarly $\gamma=0.0004$ m^{-1} is set.

Based on the parameters above the transcendental equation (4) is solved to obtain the wavenumber pair (k, l) satisfying the wavenumber selection relation shown by the dashed line in Fig. 3.

The amplitude of the disturbance corresponding to the wavenumber components is indicated with the solid line in the figure, the ordinate of which represents the relative value of the components. It can be seen from Fig. 3 that the wavenumber domain constructing the cloud streets is narrow. It starts from the cutoff wavenumber $k_c=0.00046$ m^{-1} and $l_c=0.00071$ m^{-1} . The contribution of the components might be negligible as $k>0.001$ m^{-1} , $l>0.003$ m^{-1} . Figure 4 shows the distribution of the updraft ($w>0$) close to the top of the boundary layer calculated by Eq. (5). The updraft regions align regularly. It suggests that the pattern of the cloud streets induced by the updraft motion should be similar to that in Fig. 4. The cloud street presents an angle of 20° to X

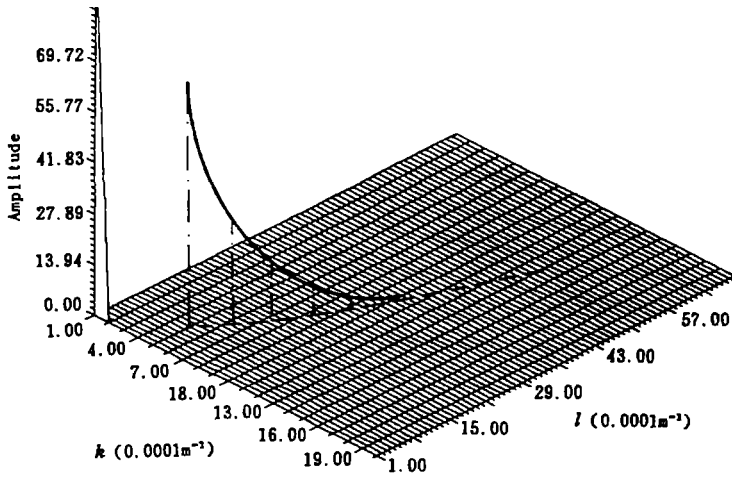


Fig. 3. The wavenumber selection relation based on the weather conditions of Station A. The axes are k and l respectively. The dashed line represents the corresponding wavenumber pair (k, l) satisfying wavenumber selection relation (4), the solid line the amplitude of the component with wavenumber of k and l . Unit of axes is 10^{-4} m^{-1} .

axis, i. e. mean wind direction in the boundary layer. The cross-wind spacing is about 7 km. Figure 5 shows the distribution of the disturbance velocities (v, w) in YZ section, i. e. cross-wind section. Within 15 km in cross-wind direction there are four vertical vortices with two clockwise and two anticlockwise. In fact they consist of two waves. The center of the large vortices is located at the top of the boundary layer, tallying with the observations taken by airplane over North Sea in KonTur Project (Brummer 1985). The

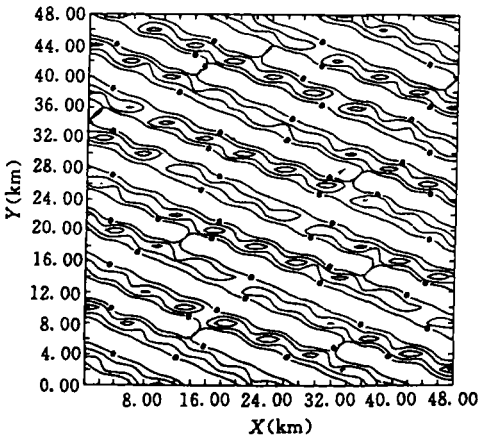


Fig. 4. Distribution of updraft ($w > 0$) at the top of the boundary layer by theoretical solution based on the weather conditions at Station A. The interval of isolines is 1 m s^{-1} .

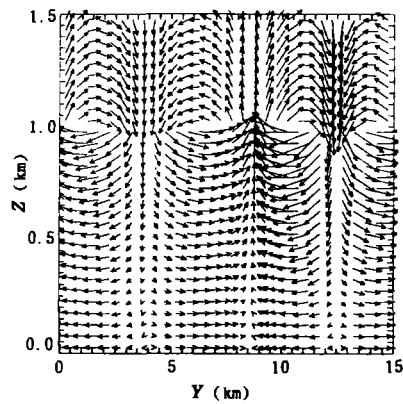


Fig. 5. Distribution of disturbance velocities (v, w) on YZ section by theoretical solution based on the weather conditions at Station A. Y axis is the cross-wind direction.

maximum updraft produced by the vortex motion also occurs near the top of the boundary layer. It is judged from Fig. 5 that the updraft may extend to high levels. The aircraft measurements over land showed (Kuettner et al. 1987) that strong vertical motion induced by convection waves could be observed at height of 9 km. These observational facts are reflected in Fig. 5.

The series of theoretical calculations above offers the patterns of the disturbances induced by the interaction between the convection and the waves. These disturbances propagate horizontally along the wavenumber vector $\mathbf{K} = ki + lj$, that is, the wave propagation direction is orthogonal to the direction of the cloud street alignment. Since the vertical extent of water vapor is confined within the boundary layer the cloud forms in the updraft region by water vapor lifting condensation: while in the downdraft region the dry air of the upper layer entrains into the boundary layer to form clear air region. Thus the cloud region and clear air region align alternately to form cloud streets.

Figure 6 shows the distribution of the interface, which may be taken as a material surface and also approximately the upper limit of the layer containing plentiful water vapor. If the raised part of the interface surpasses the lifting condensation level it may be regarded as the cloudy region. This figure may explain why the cloud bands in the streets align regularly.

2. Cold Air Transformation—Transition from Cloud Streets to Convective Cells

Station B is located at the ocean surface south of Iceland, where the cold air receives much latent and sensible heat from the warm ocean surface and transforms gradually. Thus the instability in the boundary layer decreases. And because the temperature in the boundary layer increases, the stability in the upper layer also decreases. Therefore parameters m and n decrease correspondingly. Another characteristic of this phase is the larger deviation of the wind direction between the upper and the lower layers caused by horizontal spreading of the cold air in the lower layer. According to the weather conditions at this station we have $n = 0.0003 \text{ m}^{-1}$, $m = 0.0002 \text{ m}^{-1}$, and $\alpha = 0.15$. It can be seen from

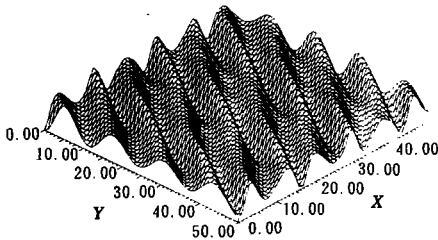


Fig. 6. Distribution of the top of boundary layer by theoretical solution based on the weather conditions at Station A.

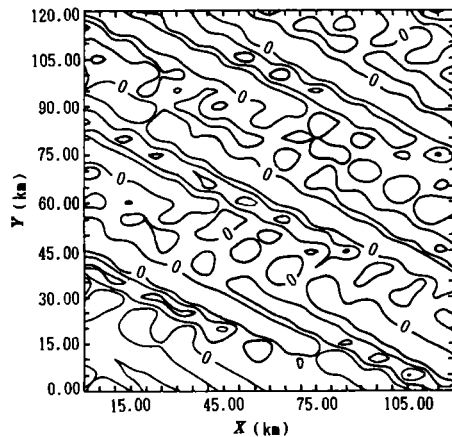


Fig. 7. As in Fig. 4. but for Station B.

the satellite picture that the streets in the phase widen gradually and change into cells ultimately. The spacing of the cloud bands is about 20–30 km.

Figure 7 shows the distribution of the vertical motions calculated according to the parameters in Station B. In comparison with Fig. 4, one of the remarkable features in this figure is the widening of the convective bands. The spacing, however, is uneven with the minimum of 20 km and the maximum of 30 km. Another feature is the discontinuity of the convective bands. Some of them have broken up into several isolated cells. In the vicinity of Station B the streets and cells appear simultaneously, see Fig. 1. This is the characteristic of the transition phase.

3. Last Phase of Convection—Convective Cells

Station C is located at Shetland Isles north of Scotland. The atmospheric conditions at the station reflect the features of the last phase of the convection. The cold air transforms further. The stratification in the boundary layer tends to be neutral and wind speed decreases and the wind direction shear between the upper and lower layers increases further. Since the trough-line of the low pressure over Norwegian Sea in Fig. 2 tilts backward, the contours at 700 hPa and 850 hPa make a large angle. Accordingly the direction shear is estimated to be $\alpha = 1$. During cold air transformation the values of potential temperature gradient, $|\partial\theta/\partial z|$, both in the upper and the lower layers decrease and the wind speeds decrease too. Because the values of parameters n and m are proportional to $|\partial\theta/\partial z|^{1/2}$ and inversely proportional to wind speed, the values of n and m still increase from Stations B to C, i. e. $n = 0.0006 \text{ m}^{-1}$, $m = 0.0004 \text{ m}^{-1}$ and $\gamma = 0.0005 \text{ m}^{-1}$. With the continuous mixing the boundary layer has deepened to be, say, $h = 1500 \text{ m}$. The convection in the satellite picture appears in cellular form. Though the cells are transformed from the cloud bands, it is hardly discerned that they align along the wind direction. The shape of the cells is approximately central-symmetric with spacing of about 30–40 km.

Figure 8 shows the wavenumber selection relation obtained according to the parameters above. The illustration of the figure is similar to that of Fig. 3. In comparison

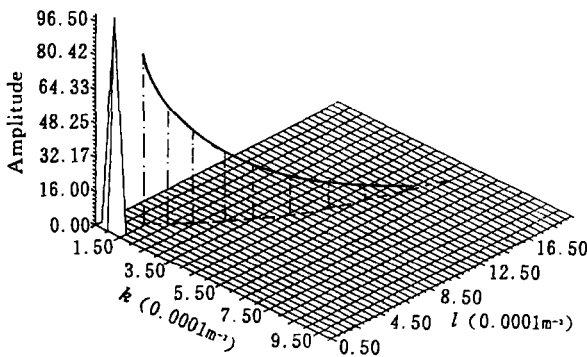


Fig. 8. As in Fig. 3, but for Station C.

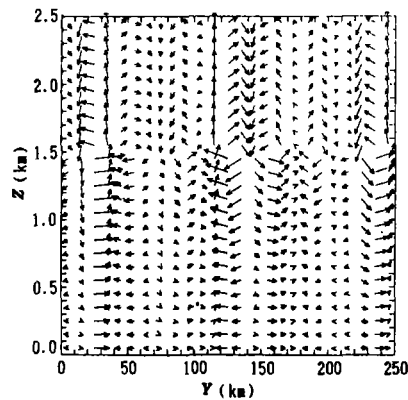


Fig. 9. As in Fig. 5, but for Station C.

with Fig. 3. however, it can be seen that the wavenumber composition of cellular convection is obviously different from that of streets. One of the differences is that the cutoff wavenumbers of the cells are much lower.

It can be known from Eq. (6) that as α gets larger, e. g. $\alpha \approx 1$, the cutoff wavenumbers k_c and l_c , satisfying relation $(k_c + \alpha l_c)^2 = m^2$ may become smaller, i. e. $k_c \approx 0.00015 \text{ m}^{-1}$ and $l_c \approx 0.00025 \text{ m}^{-1}$. This means that the maximum wavelengths L_x and L_y of the disturbances in X and Y directions respectively both increase. Another difference is that as k and l increase the amplitude of the wavenumber components decreases slowly. This feature indicates that the cellular convection consists of wider wavenumbers domain. This means that cells are different from each other since they consist of diverse wavenumber components. This characteristic is illustrated by Fig. 9, showing the distribution of velocities (v , w) in YZ section. There are several clockwise or anticlockwise vortices in the figure. These vortices have various size, spacing and strength. This reflects the multiscale structure of these vortices. There are five updraft regions with different width. The diameters of the cells in Fig. 9 are about 20 to 60 km, corresponding to the sizes of the cellular cloud clusters in the vicinity of Station C in the satellite picture Fig. 1.

4. Reestablishment of Cloud Streets over Land

Station D (London) located at the south end of England, represents the atmospheric conditions over coastal area of Europe. In the daytime of middle March the surface temperature on land is much higher than that on ocean. As the transformed cold air over ocean surface comes into land the instability of boundary layer strengthens again. In addition, since West Europe is located behind the south end of the trough mentioned previously, the wind directions in the upper layer and the lower layer tend to be consistent again. According to the atmospheric conditions it is estimated that $\alpha = 0.125$, $n = 0.0011 \text{ m}^{-1}$, $m = 0.0004 \text{ m}^{-1}$ and $\gamma = 0.0004 \text{ m}^{-1}$. It can be seen from the satellite picture Fig. 1 that as the cold air enters the warm land surface the cloud streets reappear over West Europe. Since water vapor, however, is not so rich as that over ocean the cloud bands develop imperfectly. In comparison with the first phase, the cloud bands on the satellite image are not clearly discernible. Figure 10 is the satellite picture of two days later, i. e. at 1347 GMT, March 13, 1982. Obviously, Fig. 10 and Fig. 1 represent the same process. Figure 10, however, indicates more delicately the difference of the convective process of the same air mass over ocean surface and over land surface. Over the open ocean the cells are open with diameter of about 40 km. Over the ocean next to the land, for instance over Biskay Bay, the cells widen to about 70 km and the cloud amount decreases. This means that the convection tends to weaken. After entering the land the form of convection becomes cloud streets. The variety of cloud form is obviously caused by the difference of the atmospheric conditions over the land and over the ocean.

IV. DISCUSSION

The above theoretical and synoptic analyses indicate the wave nature of the vortex motion in the convective boundary layer. This kind of disturbance caused by the interaction between convection and waves is called convection waves. It is known from

Eq. (5) that convection waves consist of different wavenumber components. Since the amplitude of the components decreases with the wavenumber the contribution to the composed disturbances mainly comes from a narrow wavenumber domain starting from the cutoff wavenumber k_c and l_c . The analyses indicate that the characteristics of the convection waves such as shape, alignment, orientation and spacing are determined by the wavenumbers in the vicinity of k_c and l_c . Equation (4) shows that the cutoff wavenumbers are determined by $\mu=0$, i. e. $m^2/(k_c + al_c)^2 = 1$. As $\mu=0$, Eq. (4) becomes

$$l_c^2 = \frac{k_c^2 + n^2}{\gamma^2} \coth^2(h) - k_c^2. \tag{7}$$

In the initial phase of cold air outbreaks the huge temperature difference between cold air and warm ocean makes the boundary layer strong unstable. The potential temperature profile is shown by the curve 1 in Fig. 11 and its counterpart simplified in the two-layer model is shown by curve 2. This profile gives large values of m and n , and therefore large values of k_c and l_c . The ratio of k/l shown in Fig. 5 is small. Therefore in the phase the convection is shaped as streets with cross-wind wavelength much smaller than downwind wavelength. The street is narrow and aligns approximately along the mean wind direction.

The potential temperature profile of the transformed cold air over warm ocean is simply illustrated by the curve 3 in Fig. 11. Its characteristics are as follows. The instability decreases, the boundary layer deepens and correspondingly the temperature jump, $\Delta\theta$, at the top of boundary layer increases as the potential temperature gradient in the upper stable layer decreases. In general, the values of m and n in the final phase are smaller than that in the initial phase. It can be seen from Eqs. (6) and (7) that the

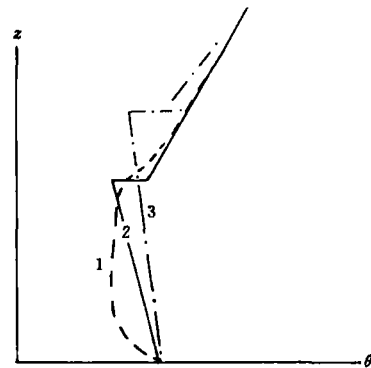
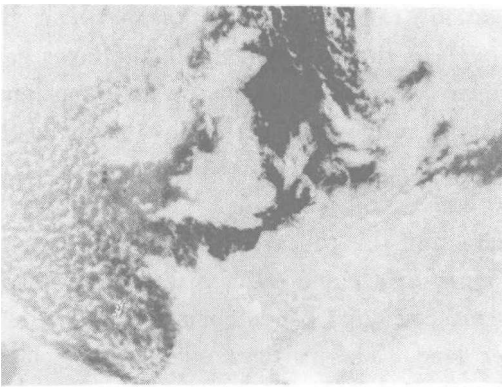


Fig. 10. As in Fig. 1. but for 1347 GMT, March 13, 1982.

Fig. 11. Potential temperature profiles in the lower atmosphere as cold air outbreaks over warm ocean surface. Dashed line represents the profile at the initial phase of the cold air outbreaks, solid line the approximate profile in the two-layer model, dot-dashed line the approximate profile after cold air transformation.

decrease of m and n , or increase of h and γ all make the cutoff wavenumbers smaller, that is, make the cross-wind spacing of the convection larger. In addition, the increase of ratio, k/l , makes the values of the cross-wind wavelength and the downwind wavelength close to each other, and the intersection angle between the convective bands and X axis tend to 45° .

Another factor causing the increase of the width of convection cells is the wind direction shear, α , between the upper and the lower layers. With the increase of α the cutoff wavenumbers k_c and l_c at the same value of m are necessarily small and the wavenumber domain constructing the disturbances therefore widens. The composition of various components makes the convective bands break and form isolated and separate cells.

So far only the situation of $k > 0$ and $l > 0$ is discussed, this is the case that the wavenumber vector \mathbf{K} points to the quadrant of $x > 0$ and $y > 0$. In fact for Eq. (4) there is also a solution of $k > 0$ and $l < 0$, in which mode \mathbf{K} points to quadrant of $x > 0$ and $y < 0$, that is, the waves propagate in the fourth quadrant. The analytical solutions (Sang 1993) indicated that as $\alpha > 0$ the amplitude of mode of $k > 0$ and $l < 0$ is much smaller than that of mode of $k > 0$ and $l > 0$; whereas $\alpha < 0$ the mode of $k > 0$ and $l < 0$ dominates. During cold air outbreaks the cold advection in the lower atmosphere makes the wind turn back, i. e. $\alpha > 0$. Thus the mode of $k > 0$ and $l > 0$ discussed above is the normal situation. Statistics show that in most cases the cloud streets align left to the mean wind direction (Atkinson 1981).

Based on the convection wave theory we have analysed a shallow convective process induced by a cold air outbreak over warm ocean. It may be understood from the previous analyses that the large vortices in CBL originate from the interaction between the convection and the waves. The roll vortices as well as the waves in the stable layer gain energy from convective instability and their patterns are determined by the wave motions, ultimately by the atmospheric conditions in the upper and lower layers. The studies of the coupling relation between CBL and the upper stable layer are of importance to understand the processes in CBL as well as the dry or moist convection processes.

The analyses above may also be appropriate for the processes over land surface. Because of the horizontal inhomogeneity of the land surface and the less water vapor, the vast, horizontally homogeneous and clearly discernible cloud bands such as cloud streets and convective cells can hardly be found over land. The vortices over land surface, however, may still be thought to originate from the interaction between convection and waves.

The interaction effects have been demonstrated in several observational and numerical studies (Kuettner et al. 1987; Clark et al. 1986). The idea of convection-wave interaction may promote the researches in atmospheric field observations, numerical simulations and fluid dynamics experiments of the roll vortices. These researches, whereas, may further illustrate the effects of some factors such as time-variation, nonlinear interaction, Coriolis force as well as viscosity on the large vortices.

REFERENCES

- Agee, E. M. (1987). An introduction to shallow convective systems. In *Cloud Dynamics*. Norwell, Mass.: D Reidel, pp. 3–30.
- Atkinson, B. W. (1981). *Meso-Scale Atmospheric Circulation*. London: Academic Press, pp. 101–120.
- Brummer, B. (1985). Structure, dynamics and energetics of boundary layer rolls from KonTur aircraft observation. *Beitr. Phys. Atmos.*, **58**: 237–254.
- Chou, S. H., Atlas, D. and Yeh, E. N. (1986). Turbulence in a convective marine atmospheric boundary layer. *J. Atmos. Sci.*, **43**: 547–564.
- Chou, S. H. and Ferguson, M. D. (1991). Heat flux and roll circulations over the Western Gulf stream during an intense cold air outbreak. *Boundary-Layer Meteor.*, **55**: 255–282.
- Clark, T. L., Hauf, T. and Kuettner, J. P. (1986). Convectively forced internal gravity waves: Results from two-dimensional numerical experiments. *Quart. J. Roy. Meteor. Soc.*, **112**: 899–925.
- Crossman, R. L. (1982). Analysis of vertical velocity spectra obtained in the BOMEX fair weather, trade-wind boundary layer. *Boundary-Layer Meteor.*, **23**: 323–357.
- Drazin, P. G. and Reid, W. H. (1981). *Hydrodynamics Stability*. Cambridge: Cambridge University Press, pp. 45–60.
- Etling, D. and Brown, R. A. (1993). Roll vortices in the planetary boundary layer: A review. *Boundary-Layer Meteor.*, **65**: 215–248.
- Lilly, D. K. (1966). On the instability of Ekman boundary flow. *J. Atmos. Sci.*, **23**: 481–494.
- Kuettner, J. P., Hilderbrand, P. A. and Clark, T. A. (1987). Convection waves: Observations of gravity wave systems over convectively active boundary layer. *Quart. J. Roy. Meteor. Soc.*, **113**: 445–467.
- Sang Jianguo (1991). On formation of convective roll vortices by internal gravity waves: A theoretical study. *Meteor. Atmos. Phys.*, **46**: 15–28.
- Sang Jianguo (1993). On the dynamics of convective waves. *Quart. J. Roy. Meteor. Soc.*, **119**: 715–732.
- Scorer, R. S. (1986). *Cloud Investigation by Satellite*. Chichester: Ellis Horwood Publishers, pp. 40–50.
- Young, G. S. (1988). Turbulence structure of the convective boundary layer. Part II: Phoenix 78 aircraft observation of thermals and their environment. *J. Atmos. Sci.*, **45**: 727–735.